Journal of Structural Geology, Vol. 1, No. 2, pp. 99 to 115.
Pergamon Press Ltd. 1979. Printed in Great Britain.

The simulation of fabric development during plastic deformation and its application to quartzite: fabric transitions

G. S. LISTER

Department of Tectonics, Geological Institute, University of Leiden, Leiden, The Netherlands

and

M. S. PATERSON

Research School of Earth Sciences, Australian National University, Canberra, Australia

(Received 26 *September* 1978; *accepted in revised form* 12 *February* 1979*)*

Abstract—Fabric transitions can arise in materials such as quartz in which more than one set of symmetrically equivalent glide systems must be considered. The external conditions, such as temperature and stress, affect the relative ability of different mechanisms to operate. Adopting the Taylor–Bishop–Hill analysis allows an approximation to the resulting effects in the choice of critical resolved shear stress (CRSS) values for glide on the different dislocation systems. Different CRSS values may be appropriate to simulating fabric development in different deformational environments.

For any specific set of CRSS values, for a particular deformation, a set of reorientation trajectories can be defined for differently oriented crystals with respect to the instantaneous stretching axes. There is a basic number of pattern types, and deformation leads to *c*-axes populating specific end-orientations.

The CRSS values on different glide systems can vary smoothly relative to one another, but abrupt changes result in the deformation fabrics at critical CRSS ratios. Quartz fabrics may thus be used to delineate regions subjected to particular conditions of temperature and strain-rate in deformed metamorphic terrains, provided that allowance can be made for other factors such as trace impurity content of quartz.

INTRODUCTION

IT IS WELL established that a polycrystalline material of a given type can develop different preferred crystallographic orientations when deformed under different circumstances even though the deformation is the same. For example, cold-rolled face-centred-cubic metals have two distinctive deformation fabrics, which can be designated as copper-type and brass-type; a change from one type to the other, often through transitional types, can occur as a result of a change in temperature of deformation (e.g. Hu & Goodman 1963, for copper), strain rate (Leffers 1968) or composition (Merlini & Beck 1955, for zinc content in brass) (Fig. 1). Similarly, Tullis *et al.* (1973) have shown that the experimental deformation of quartzite at relatively low temperatures or high strain rates gives rise to a fabric with a *c*-axis maximum parallel to the axis of shortening, and that there is a transition from this fabric to small-circle girdle fabrics as the temperature increases or strain rate decreases; both types of fabric are clearly attributable to deformation even though recrystallization appears at higher temperatures.

Geologists have also long been aware that in tectonic belts, where there is much evidence for the rocks having been plastically deformed, quartzites exhibit many distinctly different types of preferred crystallographic orientation (Sander 1950, Sahama 1936, Hietanen 1938, Fairbairn 1949, Turner & Weiss 1963, Hobbs *et al.* 1976). Many of these fabrics are thought to result directly from deformation and it is of interest to establish the factors that determine which particular deformation fabric will develop in specific situations. The experiments of Tullis *et al.* (1973) show that, even if the imposed deformation is the same, different conditions of temperature and strain rate can lead to different fabrics. It seems likely that an identical situation would hold in nature. It is therefore potentially of considerable geological importance to understand how different deformation fabrics can arise from the same type of deformation and to relate this to environmental variables.

The reasons for these various fabric transitions have not yet been clearly demonstrated. However, in deformation fabrics arising from the rotations of crystallographic axes accompanying dislocation glide within the grains, a factor of likely importance is a change in the preferred glide systems. A similar effect, involving the occurrence of $\{111\}\langle 11\bar{2}\rangle$ deformation twinning as an alternative to the usual $\{111\}\langle 1\bar{1}0\rangle$ slip, appears to underlie the copper to brass-type fabric transition in face-centred-cubic metals, and this idea is supported by the computer simulation study of Kallend & Davies (1972).

The present paper sets out in general terms how, on the basis of the predictions of the Taylor–Bishop–Hill model, change in the preferred glide systems would give rise to differences in preferred crystallographic orientation under the same deformation; it then presents simulations of some of the numerous transitions that could arise in quartzites as a result of changes in the relative ease of glide on the many known glide systems of quartz and, briefly, considers possible geological implications.

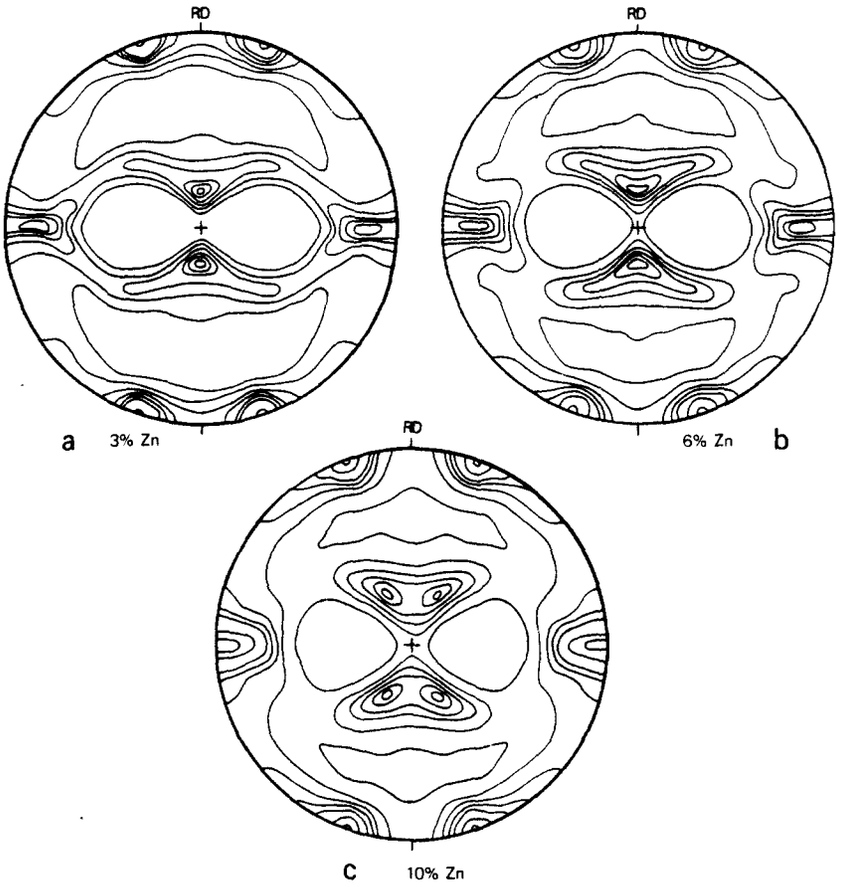

Fig. 1. (a), (b), & (c) are (111) pole figures illustrating the copper-brass fabric transition as a function of Zn-content (after Merlini & Beck 1955). The transition also takes place as a function of temperature and strain-rate. Shortening axis is vertical and the rolling direction (RD) is north–south. Rolling gives approximately plane strain.

THE TAYLOR–BISHOP–HILL MODEL AND FABRIC TRANSITIONS

A previous paper (Lister *et al.* 1978) critically reviews the Taylor–Bishop–Hill model for polycrystal behaviour and its use in simulating the development of preferred crystallographic orientation in polycrystalline material undergoing dislocation glide within the grains. In brief, the model assumes (a) that the deformation occurs within each grain and subgrain by a combination of interpenetrating glide processes, each glide system being represented by a simple shear; (b) that the gliding obeys a rigid-plastic flow law and (c) that the deformation is uniformly distributed. The nature of the fabric predicted to develop during a given imposed deformation is determined by the choice of available glide systems and by the choice of the values of the critical resolved shear stresses needed for these glide systems to become active.

Fabric transitions are therefore to be expected when the critical shear stresses on the glide systems change relative to each other sufficiently so that different combinations of glide systems can become active.

The relative contribution of the various glide systems to the deformation is thereby changed, and this causes a modification to the fabric that is developed during a simulation.

The critical resolved shear stress requirement for activity of a given glide system can be represented in stress space by a yield constraint hyperplane. When the yield constraints for all potential glide systems are considered together, a yield surface is defined. This is a piecewise continuous convex tube or hyperprism bounding all possible stress states in a grain. Stress states outside the yield surface are impossible because of the rigid-plastic flow law, while stress states on the yield surface allow the material to undergo perfectly plastic flow. For stress states inside the yield surface the material is rigid.

The Taylor and the Bishop–Hill analyses invoke optimization procedures to calculate which glide systems will act in a specified deformation. The result of these optimizations is that the actual stress state controlling the deformation lies at a vertex of the yield surface. Such vertices are defined, in general, by the intersection of the yield constraints for at least five independent glide systems (giving a vertex of rank 5). The stress states represented by these vertices can activate only the glide systems whose yield constraints intersect to form the vertices.

Thus the vertices of the yield surface determine which combinations of glide systems can be simultaneously activated to allow deformation to take place. Note that in cases of special symmetry between deformation and crystal axes, stress states represented by vertices of lower rank than 5 may suffice to accomplish the deformation, using correspondingly fewer glide systems. Conversely, the vertices determine which mechanisms are excluded from operation because their yield con-

straints lie outside the yield surface, so that sufficiently high resolved shear stresses on the systems cannot be attained. The vertices also determine which combinations of mechanisms cannot be activated, which is equally important.

It is proposed that changes in the combinations of operative mechanisms can give rise to some of the fabric transitions observed in nature. The combinations of glide systems that may operate simultaneously play a key role in determining the nature of a crystallographic fabric developed during a particular deformation history. Thus, the configuration of the yield surface, which determines which combinations can operate, is the most important factor in simulations of fabric development. If a change takes place in the configuration of the yield surface then a change will take place in the simulated fabric for a particular deformation history. This behaviour can be modelled by observing fabric transitions induced because of changes in the yield surface configurations for hypothetical quartzites, the plastic deformation of which is simulated in the computer.

This work considers fabrics produced by the simulated deformation of several of these hypothetical model quartzites, beginning in each case with an initial orientation population that is randomly distributed. Only *c*-axis fabrics are documented in the paper and additional data from selected examples will be presented elsewhere.

The distance from the origin of a particular yield constraint is determined by the relevant yield stress. Suppose that a set of critical yield stresses has been specified and that they are such as to prevent a particular mechanism set from becoming active because the respective yield constraints are excluded from the yield surface. Then, suppose that the particular yield stress is decreased continuously. At a certain value the constraints intersect the yield surface. This gives a change in the topological configuration of its vertices, and members of the formerly excluded mechanism set can now be activated.

As the yield stress for the particular set is further reduced, discontinuous modifications to the yield surface configuration continue to take place. Vertices may disappear, or be modified, or new vertices appear as the yield constraints move toward the origin. Eventually the yield constraint ceases to cause changes in the yield surface configuration, no matter how small the relative yield stress becomes (Fig. 2).

Configuration changes occur abruptly at certain ratios of the critical shear stresses of the potential glide systems. The set of vertices in each yield surface can be said to define topologically a specific yield surface configuration. There will therefore be a finite number of possible yield surface configurations, limited by the possible number of such subsets in the total set of all possible glide systems; in each case, the glide systems not included in the subset of active ones are those where yield constraint surfaces fall entirely outside the particular yield surface defined by the subset.

Figure 2 illustrates a change in yield surface configuration involving a substantial relative shift in a yield constraint as a result of unspecified change in environmental factors between the situations depicted in Figs. 2(a) and (b); in this case there is a transition from a yield surface having vertices defined by the yield constraint intersections A, B and C to one defined by A, B, E and D.

It is important to realize that these changes of configurations occur abruptly, although the critical yield values may vary smoothly. Furthermore, the changes in configuration may have minor or major effects on fabric development. If the change in yield surface configuration does not greatly affect the relative activities on various mechanisms, there will usually be a correspondingly small influence on fabric development.

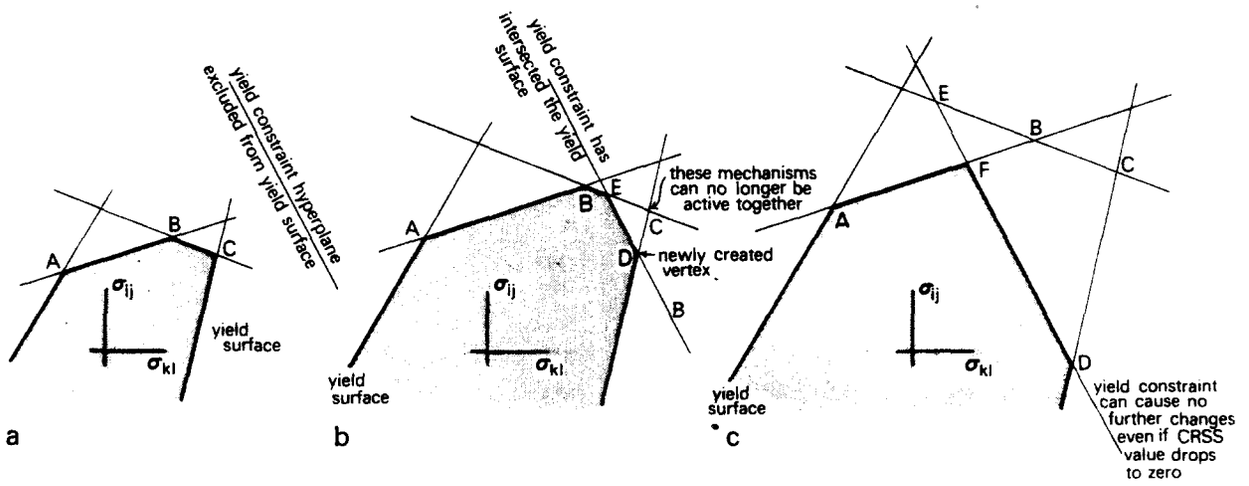

Fig. 2. (a) A yield constraint that is initially excluded from the yield surface is brought closer to the origin by continuously decreasing the CRSS value, for example as a result of changes in environmental factors. (b) The yield constraint eventually intersects the yield surface and causes a change in its configuration. (c) As the yield constraint continues to move toward the origin, vertices are created or modified, or disappear from the yield surface. There comes a point where the yield constraint can cause no further changes to the yield surface configuration even if the CRSS value is dropped to zero. The mechanism is then biased for as much activity as its geometry will allow.

THE CONCEPT OF CONFIGURATION SPACE AND ITS RELATION TO FABRIC DEVELOPMENT

Although the number of possible yield surface configurations is finite for a given material, this number may nevertheless be very large when the number of possible glide systems is large, as in quartz. It is therefore useful to have a means of representing or visualizing the whole complex of configurations and their relationships with each other, and the relative extent of the fields to which each configuration is relevant. It is convenient for this purpose to take an n-dimensional space, where each of the axes represents the value of the critical shear stress for one set of symmetrically equivalent glide systems for the material (referred to here as a symmetry set). The space is called configuration space since it can be divided into domains, the points within which represent sets of relative critical resolved shear stress values that define particular yield surface configurations. Each domain of configuration space will lead to particular types of fabric for a given deformation.

Only for simple materials is a complete description of configuration space practicable. This is because configuration space has as many dimensions as there are symmetry sets of glide systems, and it is a laborious task to examine even one yield surface configuration in enough detail to properly ascertain its properties in affecting fabric development.

In the case of quartz, when only basal, prism and rhomb systems are considered, there are 33 individual glide systems when opposite senses of glide are not distinguished, even if symmetrically distinct (Lister *et al.* 1978). Taking this grouping together with the grouping offered by the individual symmetry sets, there are eight individual independent sets of mechanisms. If the trigonal dipyramidal sets are also considered, the number rises to 11, with a total of 51 glide systems being examined. To establish all possible fabric transitions in such a material is an enormous task, beyond the available capacity of most computer facilities, and it is therefore necessary to proceed in a selective way with the aim of establishing the most important yield surface configurations for the material.

Since the aim is to establish the effects on fabric development of a set of specified glide systems, there are four approaches that might be considered.

(a) Seek to establish qualitative rules for predicting the main fabric features when particular glide systems are expected to predominate because their critical yield stresses have been made low relative to those of other glide systems. The systems are then energetically favoured for activation and will operate, as much as their geometry will allow, in relation to each particular strain situation.

(b) Assume functional relations between the critical shear stresses of the various glide systems, relating them, for example, to the lengths of the Burgers vectors or to environmental variables, and then follow a curvilinear path through configuration space to intersect all domains of distinct configurations for which these rules are obeyed. For each configuration the type of fabric for a specified deformation would then be obtained by simulation. Unfortunately, the lack of knowledge on such functional relations hinders this approach.

(c) Consider a small subset of glide systems only, so that it is possible to construct a two-dimensional section of stress space which orthogonally intersects the yield surface derived from this subset of mechanisms. The geometric form of the yield constraints can be determined in this projection, and the effects of variation of critical yield values can be studied. For simple cases, critical ratios of shear stresses can be readily determined for which changes in the configuration of this section of the yield surface take place. This approach is a useful one and is discussed in a following paper. It can only be used in the simplest cases, and it lacks generality.

(d) To proceed in a completely general fashion and consider specific, but nevertheless arbitrary, two-dimensional cross-sections of configuration space. With the help of a computer program the loci of changes in configuration of yield surfaces in this projection can be determined. Each field in the resulting diagram represents the field of relevance for a particular yield surface configuration, and the effect of the configuration on fabric development can then be characterized in any of a number of ways. The importance of individual configurations and of the various fabric transitions in the two-dimensional section is thus directly determined, and the method is extremely powerful. However, there may be a great number of possible cross-sections that can be considered important and, as already mentioned, the proper characterization of the effects of individual configurations is a laborious task. Restrictions of real time and computer facility provide the main draw-back to this method.

To describe configuration space is a lengthy procedure. We have principally used the fourth method. The problem quickly arises of how to decide which sections of the n-dimensional configuration space are most important and, when the two-dimensional section is finally obtained, which portion of it should be characterized in detail for the fabric types and fabric transitions. There is no really satisfactory way to do this, but to some extent the second approach can be used.

INDIVIDUAL GLIDE SYSTEMS AND THE EMERGING FABRIC

We now consider further the role of individual sets of symmetrically equivalent glide systems in fabric development. The question arises whether, if a given glide system has a low critical resolved shear stress (CRSS) value relative to other systems, its activity will predominate and give rise to characteristic features in the fabric which can be used to recognize this activity. For example, it has been suggested that predominant activity of basal <***a***> glide in quartz can be recognized from the nature of the fabric developed, with the basal

glide systems relatively easy to operate in comparison with other systems.

Arguments based on the predominating influence of individual glide systems have been exploited by various workers (e.g. Bhattacharyya & Pasayat 1968, Wenk *et al.* 1973, Bouchez 1977). Such analyses generally attempt to relate the fabric characteristics, especially rotationally stable end-orientations, to the behaviour of single crystals. They draw on the observations that, for example, in an isolated single crystal undergoing slip on a single plane in uniaxial compression between flat frictionless pistons, the pole to the slip plane tends to rotate towards the shortening axis. In uniaxial extension of a long thin crystal the slip direction rotates toward the extension axis. When multiple slip occurs on crystallographically equivalent systems, the rotations tend to be towards orientations that symmetrically dispose the active planes with respect to the deformation axes.

However, in carrying over these considerations to the polycrystalline situation, such as in quartzite, there are several complicating factors.

(a) The individual crystal is no longer free of lateral boundary constraints and must undergo a deformation that is compatible with that of the surrounding crystals. In this application of the Taylor analysis, compatibility is ensured by the assumption of homogeneous deformation, which introduces the Von Mises requirement of five independent slip systems if crystals undergo general strains. The existence of these lateral constraints immediately invalidates the strict application of models which apply the rotation trends shown by isolated crystals to the polycrystalline situation, and raises the question in general of the extent to which rotation trends will be affected by activity of other deformation mechanisms as required for intra-granular strain compatibility.

(b) The active glide systems that are required to accomplish the deformation may not all be symmetrically equivalent. Hence relative CRSS values enter into consideration in the selection of the active glide systems. However, it cannot be assumed *a priori* that, if one set of glide systems is assumed to have significantly lower CRSS than all other sets, the glide system in the set oriented for highest resolved shear stress will be the most active glide system. This is commonly true but the relative activity of the various systems depends strongly on the geometry, and a low CRSS value implies only that the system is biased for as much activity as the geometry of the situation will allow. The activity of the system is determined by the orientation of the grain in relation to the imposed strain increment, by which glide systems are simultaneously active to allow this strain increment, and by the type of strain increment. There may be no changes in relative mechanism activity over quite significant ranges of relative CRSS values.

(c) At moderate strains, the orientations of many of the crystals will not yet have become close to their end-orientations. The fabric will therefore also tend to reflect intermediate stages in the reorientation of crystal axes towards end-orientations. Thus, the preferred orientations actually observed will depend on the relative rates of rotation, as well as on the directions and end positions for these rotation paths.

The pattern of reorientation trajectories of the crystal axes is therefore the most important determinant of the developing crystallographic fabric, and more important than the actual end-orientations themselves. The trajectories determine not only what the fabric will be after large strains, but also how it will develop from given initial orientation distributions. In this connection, inverse rotation diagrams (Lister *et al.* 1978) have fundamental importance since they contain the basic information from which reorientation trajectories can be reconstructed. Calnan & Clews (1950, 1951a, b), attempted to derive reorientation trajectories by qualitative arguments and to infer from them the nature of resulting patterns of preferred orientation. Their arguments were based essentially on isolated crystal behaviour, somewhat modified by the concept that the principal stress axes will tend to be reoriented as rapidly as possible within each grain so that the critical shear stress is achieved simultaneously on a large number of glide systems. In the present study we obtain reorientation trajectories quantitatively derived using the Taylor–Bishop–Hill model for specific deformations.

Experience with model quartzes shows that the pattern of reorientation trajectories can be quite complex. The paths do not in general follow great circles but can be markedly curved, and even the sign of curvature may change along the path. A given reorientation trajectory may be entirely within a sub-area or domain in the inverse pole figure, this domain having a boundary that is not crossed by any of the reorientation trajectories lying within it. The possibility of multiple end-orientations also follows as a corollary of the existence of these domains.

The relative rates of reorientation can vary widely. As a result some areas of the inverse pole figure may be practically cleared of points after relatively small strains, while adjacent areas correspondingly develop concentrations. Some of these concentrations may be transient, resulting from variation of rotation rate or from convergence of the reorientation trajectories, rather than from approach towards a rotationally stable end-orientation. For these reasons it is inadequate to discuss fabrics purely in terms of end-orientations, especially at moderate strains.

The end-orientations that do develop in the fabric simulations using the Taylor–Bishop–Hill analysis are commonly found in fact to be one of the two general types already mentioned in connection with isolated single-crystal behaviour; either putting an easily activated glide system into an orientation unfavourable to its further operation or disposing the most active glide systems symmetrically in relation to the deformation axes. Apart from rotationally stable end-orientations a situation can also be approached in which the crystal axes continuously gyrate (Lister *et al.* 1978, fig. 4).

The consideration of fabric transitions can therefore be reduced to determining distinctive changes in the

topology of the patterns of reorientation trajectories as the relative CRSS values for different glide systems are varied. Sometimes the changes are extensive. In other cases the changes may be confined to small areas in the inverse rotation diagram. However, even in this second case, quite extensive changes in the inverse pole figure may follow after substantial deformation.

APPLICATION TO FABRIC TRANSITIONS IN QUARTZITE

In considering fabric transitions in a specific material, it is first necessary to list all the glide systems to be considered. However in the case of quartz, the glide systems that operate in nature are not well known and laboratory studies are still rather inadequate. Therefore we have selected a limited group of systems (Table 1) which will serve to demonstrate some of the fabric transitions that are predicted by the Taylor–Bishop–Hill theory. Note:

Table 1. Glide systems used in this study. Miller indices are used, referred to the a_1, a_2 and c-axis of a hexagonal unit cell

	Glide plane			Slip direction			Label
	0	0	1	1	0	0	a_1
Basal	0	0	1	0	1	0	a_2
	0	0	1	−1	−1	0	a_3
	−1	0	0	0	1	0	a_1
Prism	0	1	0	1	0	0	a_2
	1	−1	0	−1	−1	0	a_3
	0	1	1	1	0	0	a_1
(−) Rhomb	−1	0	1	0	1	0	a_2
	1	−1	1	−1	−1	0	a_3
	0	1	1	0	−1	1	$c - a_2$
	0	1	1	−1	−1	1	$c + a_3$
	−1	0	1	1	1	1	$c - a_3$
(−) Rhomb	−1	0	1	1	0	1	$c + a_1$
	1	−1	1	−1	0	1	$c - a_1$
	1	−1	1	0	1	1	$c + a_2$

(a) Only the (−) rhomb systems have been studied in detail here. The case of the (+) rhomb in place of the (−) rhomb may be obtained simply by a mirror reflection across the plane containing c and a in the inverse pole figure. Results for other systems will be summarized elsewhere.

(b) The CRSS values for opposite senses of shear have been considered equal for this work, regardless of whether or not this is demanded by symmetry.

A computer program was prepared to help with the difficult task of constructing two-dimensional sections of n-dimensional configuration spaces. The program delineates the boundaries across which changes in yield surface configuration occur. Then a technique which we term growth parameterization was used to determine parameters and extents of the configuration change boundaries. If the technique is applied in the correct manner and enough *cpu* time is available most fabric transitions will be detected by this method. If a configurational change affects only a very small subset of orientations it could escape attention, but in this case one can safely assume such boundaries to be unimportant.

Once a transition diagram has been prepared it remains only to characterize the individual yield surface configurations, each configuration occupying one polygonal domain on the diagram. Often there are a considerable number of configurations to be examined. It requires least effort to calculate inverse rotation diagrams for this purpose, but one should be aware that some configurations, identical under axially symmetric shortening, produce different fabrics when subjected to progressive plane strain.

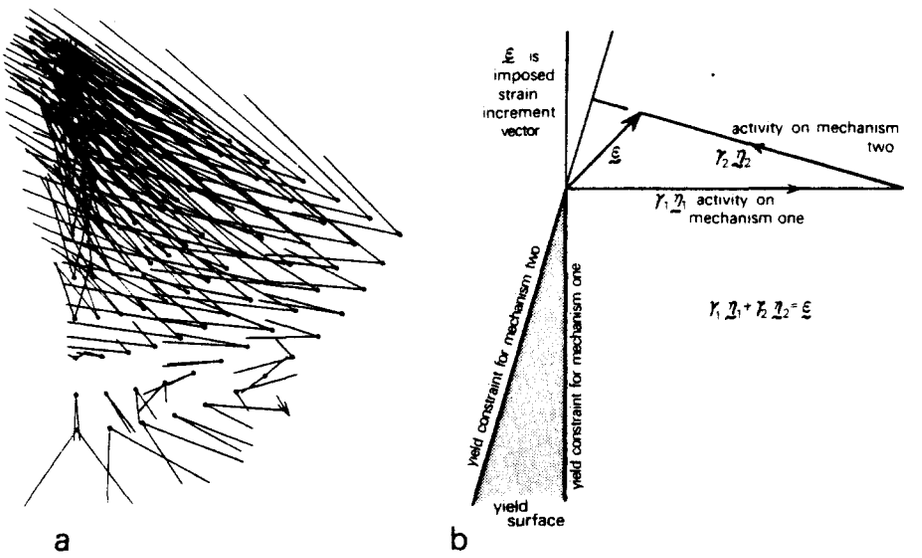

Fig. 3. Hypersensitive behaviour occurs when large rotations are predicted by the analysis for small strains. (a) An inverse rotation diagram illustrates the phenomenon. Lattice rotations are calculated for a 10% axially symmetric shortening, accommodated by the (−) rhomb <c + a> systems alone. (b) The phenomenon results when vertices of the yield surface have considerable angularity and, in consequence, mechanism activity must be high in comparison with the magnitude of the imposed strain increment.

ROLE OF THE SYSTEMS WITH <c + a> BURGERS VECTOR

A crystal of quartz deforming solely by slip can only undergo certain types of strain with respect to crystal axes if only glide systems with <a> and <c> Burgers vectors operate. General strains cannot be achieved unless at least one of the active glide systems has a slip direction and slip plane oblique to both **c**- and **a**- axes. Systems such as the (−) rhomb <c + a> systems fulfil this requirement, and there are five independent glide systems in this symmetry set alone. Paterson(1969) mistakenly listed only three independent systems because only one of the two glide directions in each glide plane was taken into account.

Simulations of fabric development with the Taylor–Bishop–Hill analysis are only possible with the glide systems listed if <c +•a> systems are not excluded from operation. This arises because the yield surface is not bounded in all directions normal to the hydrostatic stress axis unless these systems are included. However, when one set of rhomb <c + a> systems defines the yield surface by itself, a phenomenon termed 'hypersensitivity' is observed (Fig. 3a). For only small strain increments very large rotations of the crystal axes take place. Rotations of 6–8° for each percent shortening are predicted. The phenomenon is caused by some of the vertices of the yield surface having marked angularity, so that there is high activity on glide systems but the resulting strains almost cancel out (Fig. 3b). Hypersensitivity causes computational problems.

Another effect related to hypersensitivity is seen when <a> and <c + a> systems operate in conjunction. The CRSS values on the <a> systems have to be several times higher than the CRSS values on the <c + a> systems before they are excluded from the yield surface, and thus from operation. These effects arise because the <c + a> systems are not geometrically suited to accommodate strain in particular orientations.

Because the <c + a> systems are geometrically necessary to allow general strains, it is not possible to exclude them from operating during computer simulations. The <c + a> systems can be made one thousand times more difficult than any other system but they will still operate. Even if the CRSS value is set so that the <c + a> systems have minimum activity, the end-orientations that develop still reflect their influence. For example, a 25° girdle formed during axially symmetric shortening disposes the rhomb $\{10\bar{1}1\}$ and $\{01\bar{1}1\}$ planes symmetrically with the basal {0001} systems, equally inclining them to the axis of shortening. When <c + a> systems with glide planes more steeply inclined to the **c**-axis are used (e.g. the trigonal dipyramids $\{2\bar{1}\bar{1}1\}$) then the result is small-circle girdles with correspondingly greater opening angles. High strength of <c + a> systems in this analysis leads to stress heterogeneity. In reality, the material surrounding any particular grain would not be strong enough to provide constraint sufficient to withstand large stress gradients. Heterogeneous strain would help to circumvent the problem, for example by kinking or allowing hard grains to remain as relatively undeformed augen, so that difficult glide systems need not operate.

Evidence to date regarding the existence of the <c + a> Burgers vector comes mainly from experiments and is reviewed by Morrison-Smith *et al.* (1976) and Lister *et al.* (1978). Twiss (1976) suggests <c ' 2a> dislocations from slip trace data. Theoretical considerations about the large amount of non-core elastic energy involved seem to argue against such dislocations, but the relevance of such arguments to silicates is not clear.

The inclusion of the <c + a> systems constitutes a point of difficulty in assessing the relevance of this application of the Taylor–Bishop–Hill model. Certainly, in considering alternative models, heterogeneity of deformation must be one of the factors studied from the point of view of relaxing the necessity to invoke 'hard' glide systems in order to fulfil the Von Mises requirement. Other deformation mechanisms, such as dislocation climb (Paterson 1969), may also be included.

COMPETITION BETWEEN <c + a> AND <a> SYSTEMS

Competitions between systems with <a> and <c + a> Burgers vector always occur when using the Taylor–Bishop–Hill analysis, so these competitions are of first interest.

Basal <a> against (−) rhomb <c + a> systems

The first fabric transition takes place when the basal systems have a CRSS value 4.1486 times that for the rhomb <c + a> systems.

Significant effects are absent until the next transition

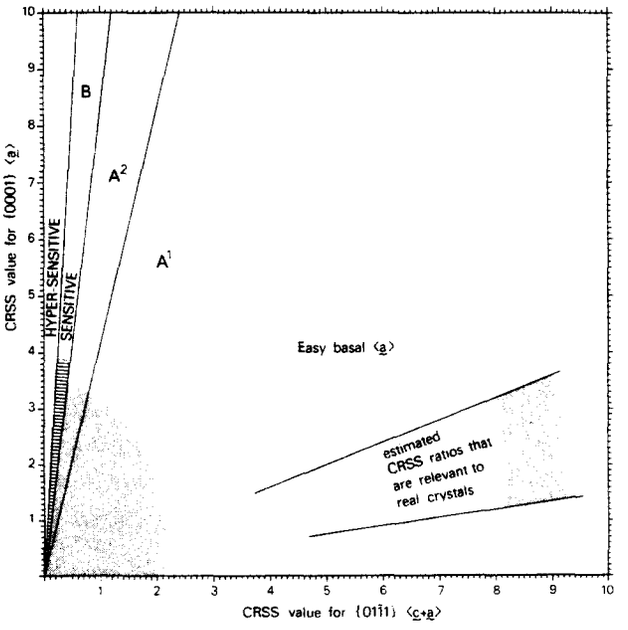

Fig. 4. Transition diagram for the {0001} <a> and $\{01\bar{1}1\}$ <c + a> systems. Fabric transitions take place at critical CRSS ratios. When basal systems are excluded from the yield surface, hypersensitive behaviour results. Configurations A^1 and A^2 are almost identical. Ornamented areas represent similar configurations.

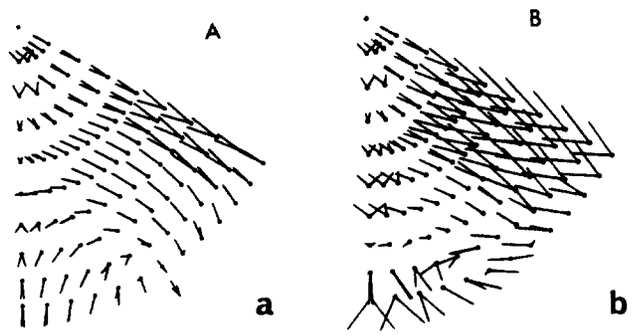

Fig. 5. Inverse rotation diagrams for 10% axial shortening illustrate reorientation trajectories for configurations A^1 (a) and B (b) of Fig. 4. When these configurations are applied to model quartzites subjected to axially symmetric shortening, point maxima of c-axes develop about the axis of shortening. The upper hemisphere of an equal-area projection is used, with positive forms on the left. In these and other diagrams the dot represents the orientation and the strokes the tangents to the reorientation trajectories. Rotations for 10% axial shortening are shown.

at a CRSS ratio of 8.2973 (Fig. 4). Basal systems are excluded at a CRSS ratio exceeding 16.595, and then hypersensitive behaviour results. Inverse rotation diagrams have been prepared for axial symmetric shortening for each of these regions (Fig. 5). Regions A^1 and A^2 are almost identical. Configuration B is sensitive and high rates of rotation are predicted.

Prism $\{10\bar{1}0\}\langle a\rangle$ *against (−) rhomb* $\{01\bar{1}1\}\langle c+a\rangle$ *systems*

Competition of prism $\langle a\rangle$ systems against rhomb $\langle c+a\rangle$ systems leads to a similar pattern of transitions (Fig. 6). The first transition occurs at a $\langle a\rangle/\langle c+a\rangle$ CRSS ratio of 1.934 but no significant effect results. Again, at the second transition (CRSS ratio 2.7473) an important change occurs, as seen in the inverse rotation diagrams (Fig. 7). A minor change takes place at CRSS ratio 6.5313 and, finally, prism $\langle a\rangle$ systems are excluded from operation when CRSS ratios exceed 9.2788. Hypersensitive behaviour then ensues.

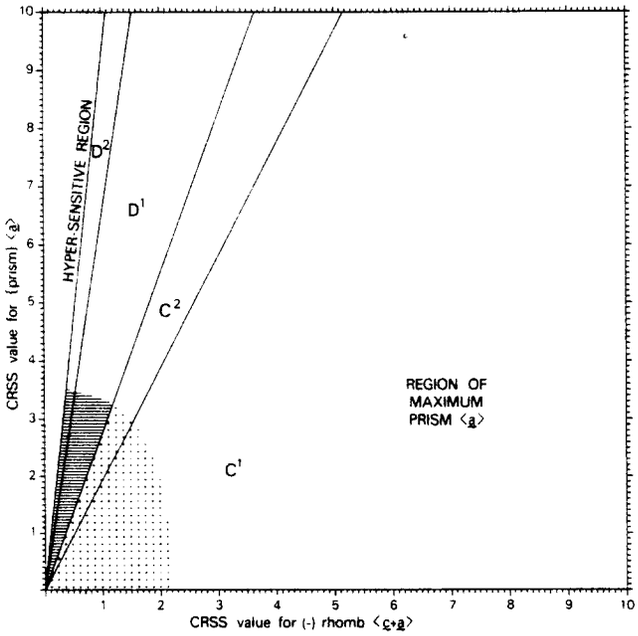

Fig. 6. Transition diagram for the $\{10\bar{1}0\}\langle a\rangle$ and $\{01\bar{1}1\}\langle c+a\rangle$ systems. Ornamented areas represent similar configurations.

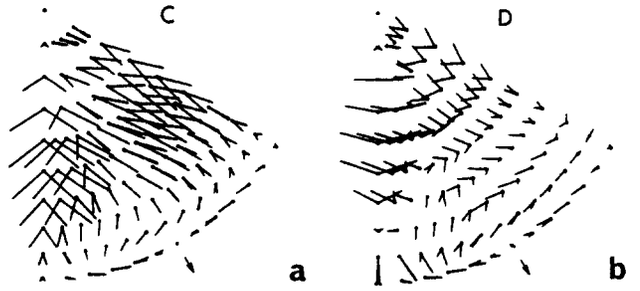

Fig. 7. Inverse rotation diagrams for 10% axially symmetric shortening for configuration C^1 (a) and for configuration D^1 (b) illustrate the two basically different patterns of reorientation trajectories for the transition diagram in Fig. 6.

(−) rhomb $\{01\bar{1}1\}\langle a\rangle$ *against (−) rhomb* $\{01\bar{1}1\}\langle c+a\rangle$ *systems*

The results of the competition between rhomb $\langle a\rangle$ and $\langle c+a\rangle$ systems are rather unusual (Fig. 8), as are the effects of rhomb $\langle a\rangle$ glide on the whole. Although transitions take place at $\langle a\rangle/\langle c+a\rangle$ CRSS ratios of 1.4867 and 2.9738, no effects can be observed in the inverse rotation diagram for each of the three yield surface configurations. They are all hypersensitive and identical to the inverse rotation diagram for the $\langle c+a\rangle$ systems alone (Fig. 3a). This is probably because the

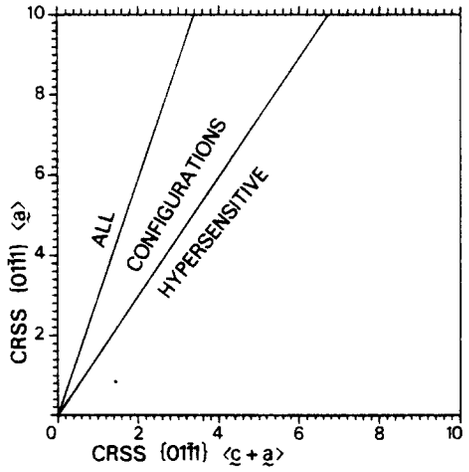

Fig. 8. Transition diagram for the competition between $\{01\bar{1}1\}\langle a\rangle$ and $\{01\bar{1}1\}\langle c+a\rangle$ systems. All the CRSS give rise to hypersensitive yield surface configurations.

rhomb $\langle a\rangle$ systems have a particular geometrical relation to the rhomb $\langle c+a\rangle$ systems. The strains (and lattice rotations) are related thus:

$$\gamma_1 \boldsymbol{E}_1 - \gamma_1 \boldsymbol{E}_2 = \gamma_3 \boldsymbol{E}_3,$$

where γ_1 and γ_3 specify the activities on the $\langle c+a\rangle$ and $\langle a\rangle$ systems, respectively, and where $\boldsymbol{n}$ is the glide plane normal, and $\boldsymbol{l}$ the slip direction:

$$\boldsymbol{E}_1 = \tfrac{1}{2}(n_i l_j + n_j l_i)_1 \text{ for } (01\bar{1}1)\,[\boldsymbol{c}+\boldsymbol{a}_3],$$
$$\boldsymbol{E}_2 = \tfrac{1}{2}(n_i l_j + n_j l_i)_2 \text{ for } (01\bar{1}1)\,[\boldsymbol{c}-\boldsymbol{a}_2],$$
$$\boldsymbol{E}_3 = \tfrac{1}{2}(n_i l_j + n_j l_i)_3 \text{ for } (01\bar{1}1)\,[-\boldsymbol{a}_1].$$

These linear dependence relations arise because there are three possible slip directions in each slip plane.

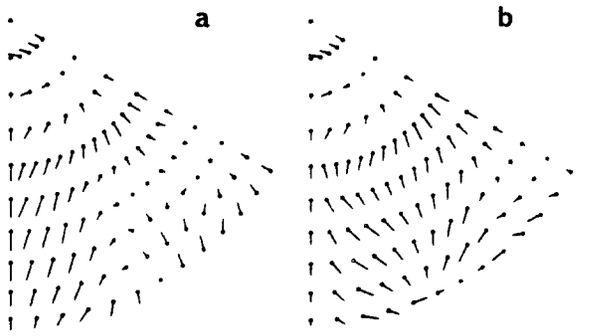

Fig. 9. (a) A model simulation for prism <c> and (−) rhomb <c + a> systems, CRSS ratio 1:3, for axially symmetric shortening produces a c-axis girdle inclined 65° to the shortening axis and the inverse rotation diagram. (b) Addition of prism <a> to the competition, with a CRSS value equal to that on the <c> systems, results in inverse rotation diagram. A seemingly minor change to the reorientation trajectories has taken place, but this causes a big change in the developed fabrics. For plane strain a maximum of c-axes now forms about the axis of extension, and for axial shortening a-axes align parallel to the axis of shortening. Thus a fabric typical of prism <c> glide forms only with prism <a> glide, indicating that use of simple end-point criteria is not possible with the Taylor–Bishop–Hill analysis.

Analogous effects occur with the prism <a> and <c> systems, and the prism <c + a> systems.

Further aspects of the influence of prism <a> systems

It is now convenient to consider the influence exerted by prism <a> systems on fabric development. These systems often have very high activity in the majority of grain orientations, without seeming to affect the fabric that develops or, at least, affecting the fabric that develops in a subtle fashion only. Often end-orientations are populated that reflect the influence of other glide systems more difficult to activate.

These effects arise because of the unusual geometry of prism <a> systems. They are systems difficult to align in unfavourable orientations for continued operation, and because of their cylindrical geometry have a distinct tendency to start the crystallographic axes gyrating. Because this is so, end-orientations more characteristic of other systems tend to be populated, compromising the overall rate of energy dissipation by minimizing activity on other systems. The predictions of the Taylor–Bishop–Hill analysis are at variance with those of the model of Calnan and Clews as, as applied by Bhattacharrya & Pasayat (1969), because of these phenomena.

ROLE OF THE PRISM <c> SYSTEMS

Prism <c> glide with difficult (−) rhomb $\{01\bar{1}1\}$ <c + a> glide results in a maximum concentration of c-axes 65° from Z, for axial shortening (Fig. 9a). This end-orientation aligns prism and rhomb planes symmetrically to the shortening axis. However, when prism <a> glide is allowed (Fig. 9b) a maximum forms at high angles to the axis of shortening. The end-orientation populated places prism <c> in the orientation most unfavourable for continued operation, and the fabric by simple criteria might be classified as characteristic of prism <c>. By the same token, the influence of prism <a> is not visible. Because of a small adjustment in the pattern of reorientation trajectories a large change in the pattern of preferred orientation develops.

The competition between basal <a> and prism <c> systems has an important effect on fabrics because the rotations produced by the basal systems are in exactly the opposite sense to the rotations that result when the prism systems operate. Basal systems rotate the c-axis towards the axis of shortening. Prism <c> systems lead in many cases to c-axis maxima near the axis of extension. When both systems operate simultaneously diffuse c-axis fabrics tend to result.

COMPETITION BETWEEN BASAL AND PRISM <a> SYSTEMS

Competition between individual <a> systems and various <c + a> systems is easy to document and discuss. However, implicit in a discussion concerning basal <a> and (−) rhomb <c + a> systems is an assumption that the rhomb or prism <a> systems have high CRSS values. This might not be a reasonable assumption, thus competitions between many systems at a time must be considered if 'realistic' portions of configuration space are to be examined.

First, the competition of the (−) rhomb <c + a> systems with {0001} <a> and $\{10\bar{1}0\}$ <a> systems is considered. This section is extremely complex and extends a considerable distance from the origin before regaining the simplicity present in the competitions between only one <a> glide system set and one <c + a> set. The transitions discovered by Chin & Mammel (1970) form only a subset of the total. The configurations closest to the origin give rise to the fabrics in which the basal and prism <a> glide systems are most significant.

There are several points that may be understood about these diagrams. Firstly, they show that if the yield stress on either of the <a> glide systems is increased, then eventually it is excluded from operation. In these sections of configuration space the only transition boundaries are lines parallel to the axis, indicating transitions involving the other <a> system with the <c + a> system. A great deal can be learnt about the way vertices behave on the yield surface. For example, points where several transition boundaries converge define CRSS values which activate many dislocation systems simultaneously.

The pattern of fabric transitions for this competition is summarized by showing it on simplified transition diagrams, the c-axis pole figures for axially symmetric shortening (Fig. 10a) as well as for plane strain (Fig. 10b). One point is that, for plane strain, c-axis fabrics form with maxima at the γ-axis, for a particular group of configurations. This end-orientation is commonly attributed to the influence of prism <a> systems. However, as can be seen, prism <a> systems are rather difficult and at the next transition boundary they are excluded from operation.

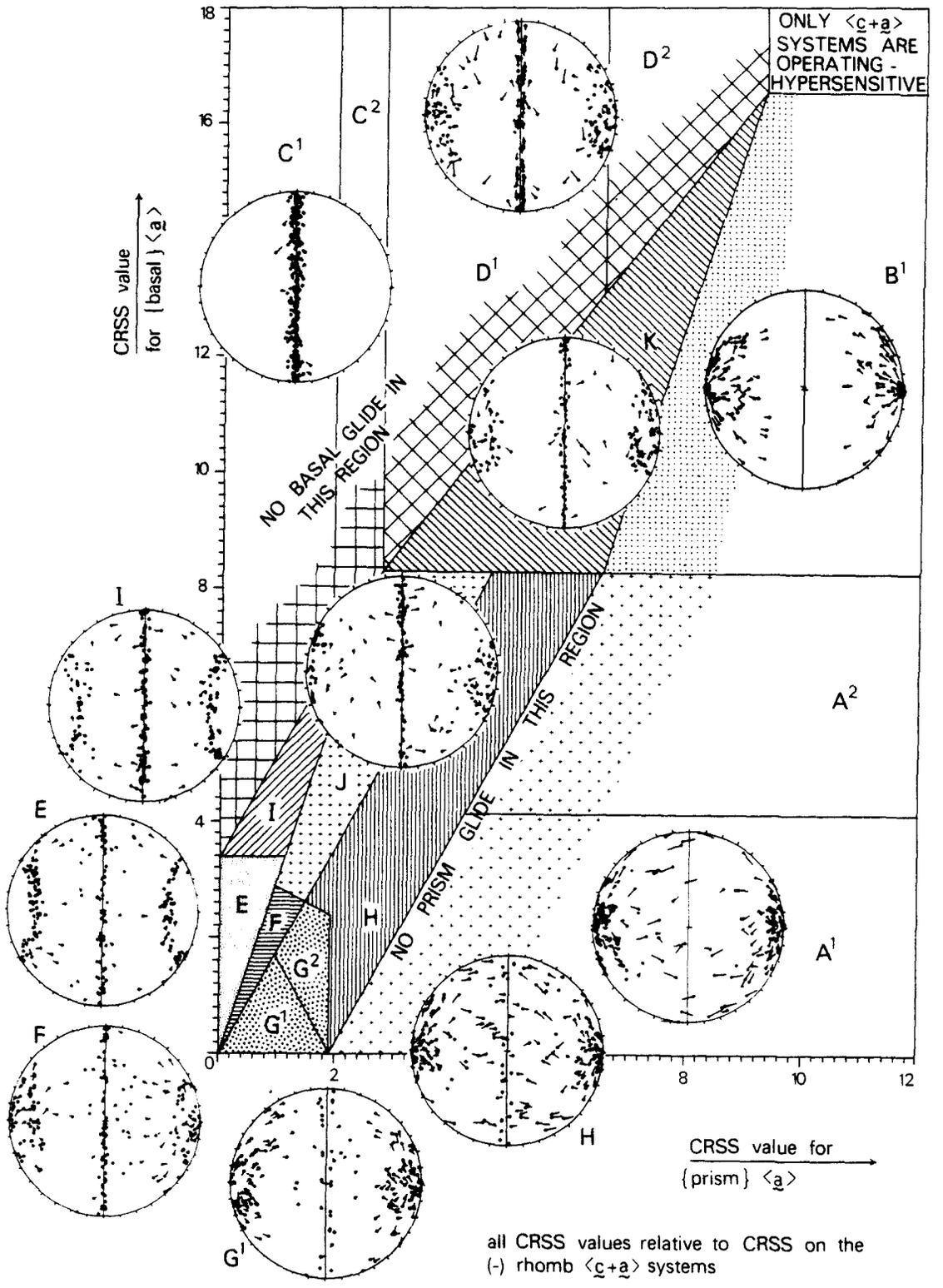
ONLY ⟨c+a⟩ SYSTEMS ARE OPERATING - HYPERSENSITIVE
NO BASAL GLIDE IN THIS REGION
NO PRISM GLIDE IN THIS REGION
CRSS value for {basal} ⟨a⟩
CRSS value for {prism} ⟨a⟩
all CRSS values relative to CRSS on the (-) rhomb ⟨c+a⟩ systems
C1
C2
D1
D2
B1
K
I
J
E
F
G1
G2
H
A1
A2
0
2
4
8
10
12
16
18

Fig. 10(a)

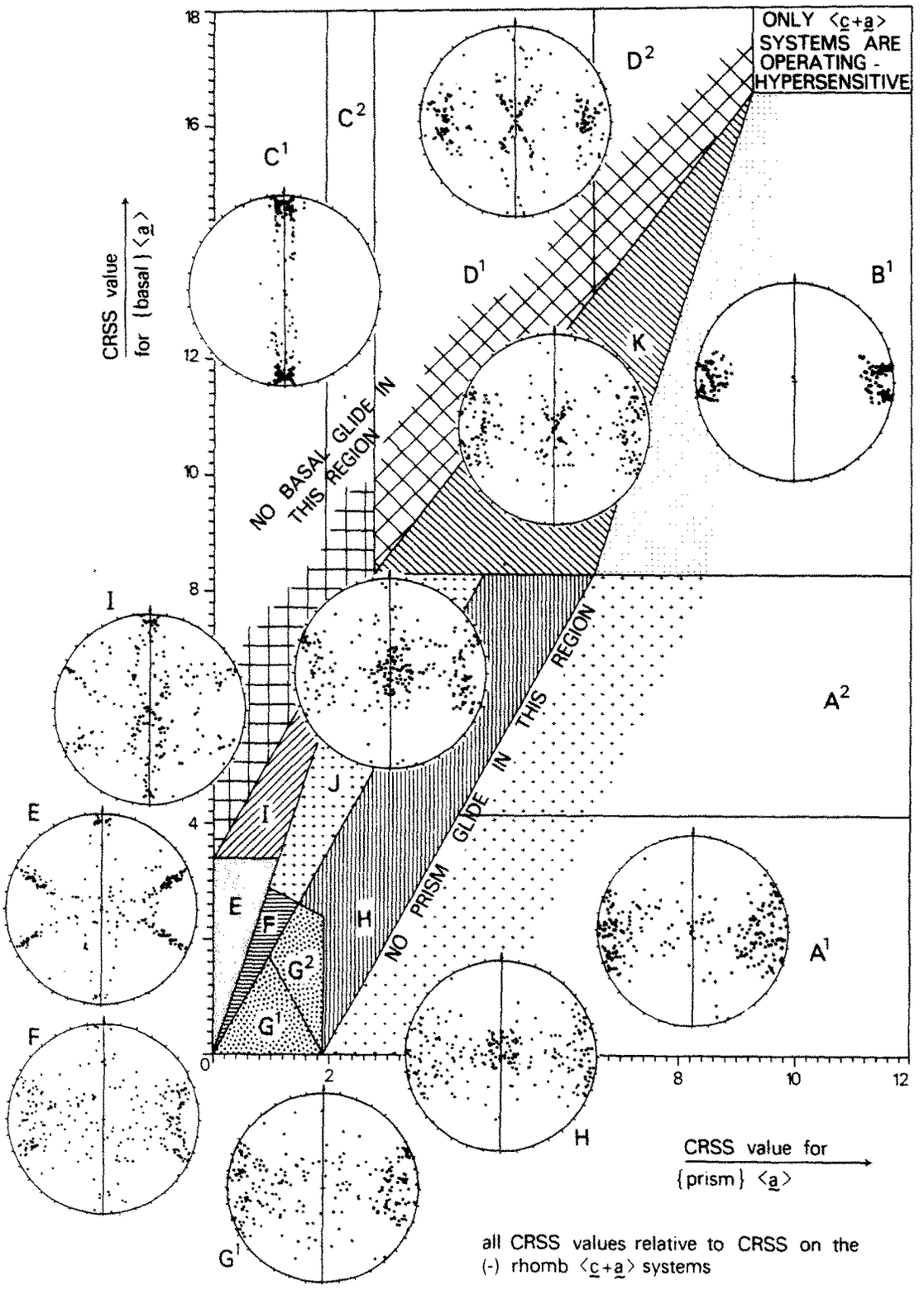

Fig. 10(b)

Fig. 10. Transition diagram for the {0001} <*a*>, {10$\bar{1}$0} <*a*> and (−) rhomb <*c* + *a*> systems. This diagram extends a considerable distance from the origin before either of the <*a*> mechanism sets is excluded and the simplicity of two-dimensional competition between one set of <*a*> mechanisms and the <*c* + *a*> systems is regained. The pattern of fabric transitions is illustrated for model quartzites of 250 grains subjected to 65% shortening in (a) axially symmetric shortening or in (b) plane strain. The axis of shortening is horizontal for each diagram and the extension axis is vertical. Pole figures are on the lower hemisphere equal-area projection. The same applies to the layout for the following diagrams. Only *c*-axis pole figures are shown. The axis of shortening is E–W and the axis of extension is N–S.

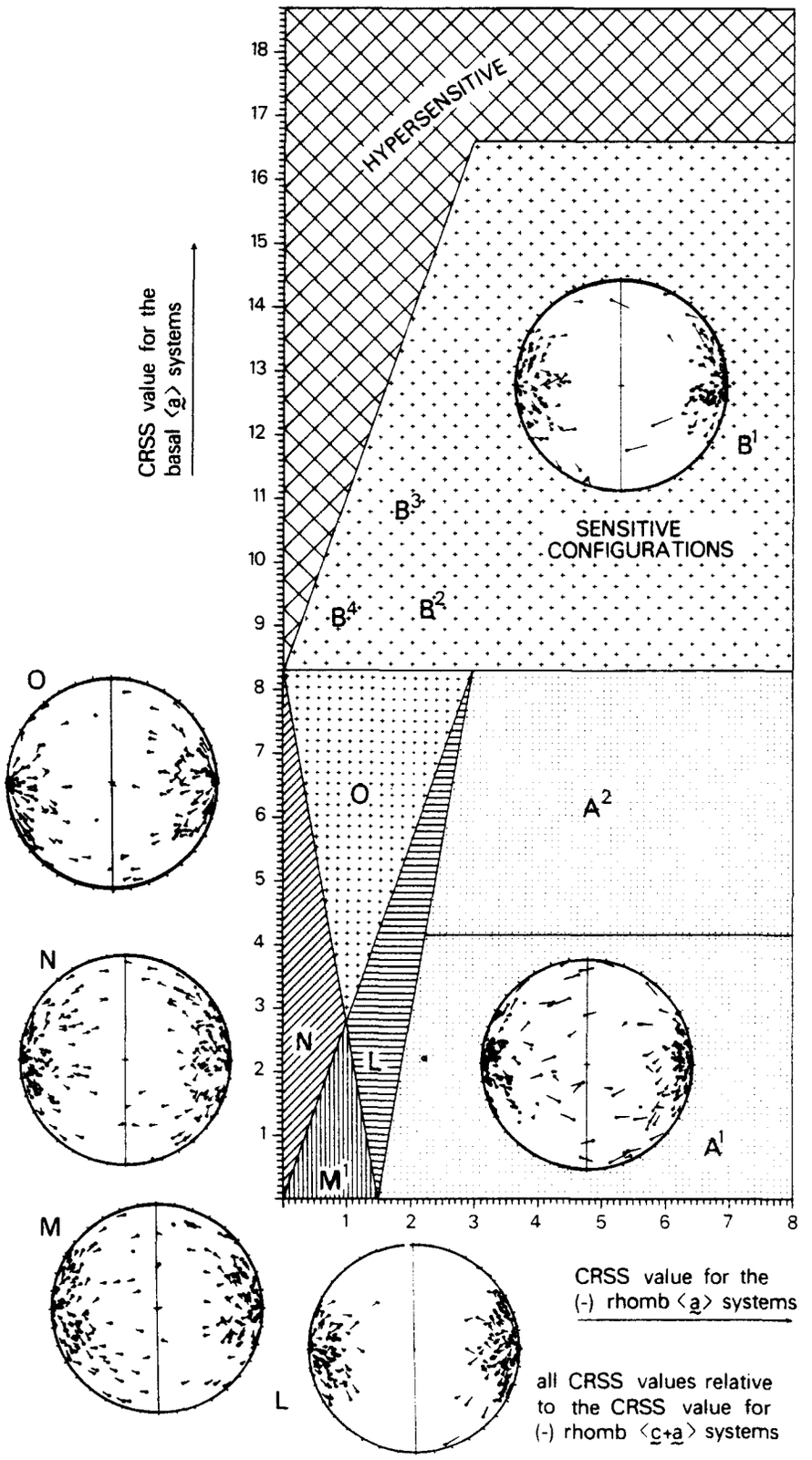
HYPERSENSITIVE
SENSITIVE CONFIGURATIONS
CRSS value for the basal ⟨a⟩ systems
CRSS value for the (-) rhomb ⟨a⟩ systems
all CRSS values relative to the CRSS value for (-) rhomb ⟨c+a⟩ systems
B1
B2
B3
B4
A1
A2
O
N
M
L
M1

Fig. 11(a)

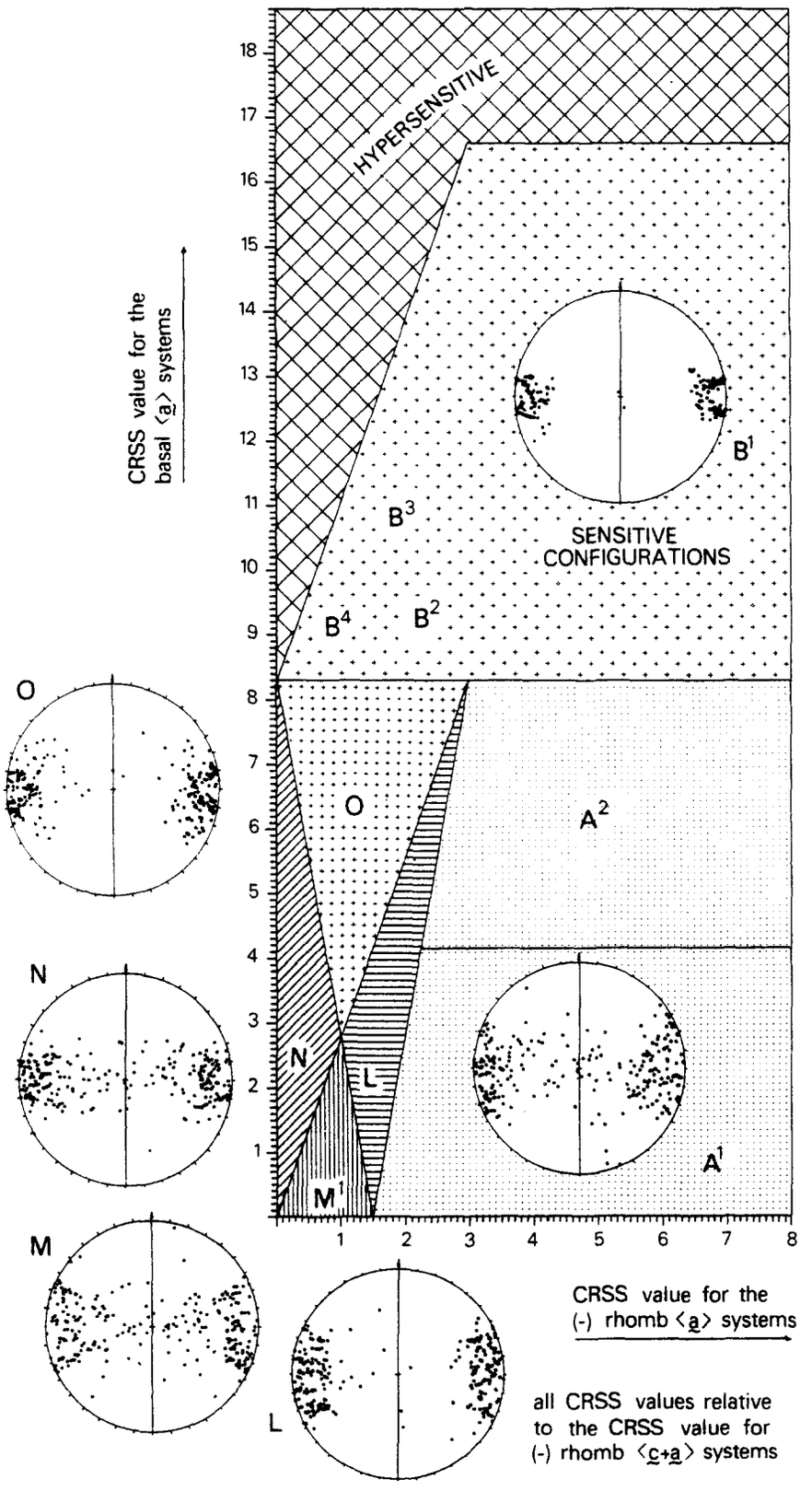

Fig. 11(b)

Fig. 11. Transition diagram for the competition between {0001} <*a*>, {01$\bar{1}$1} <*a*> and {01$\bar{1}$1} <*c* + *a*> systems. The most important domains are shown. Model quartzites consisting of 250 grains have been subjected to 65% shortening in (a) axially symmetric shortening and in (b) plane strain to illustrate the fabric transitions. Only *c*-axis pole figures are shown as for Fig. 10.

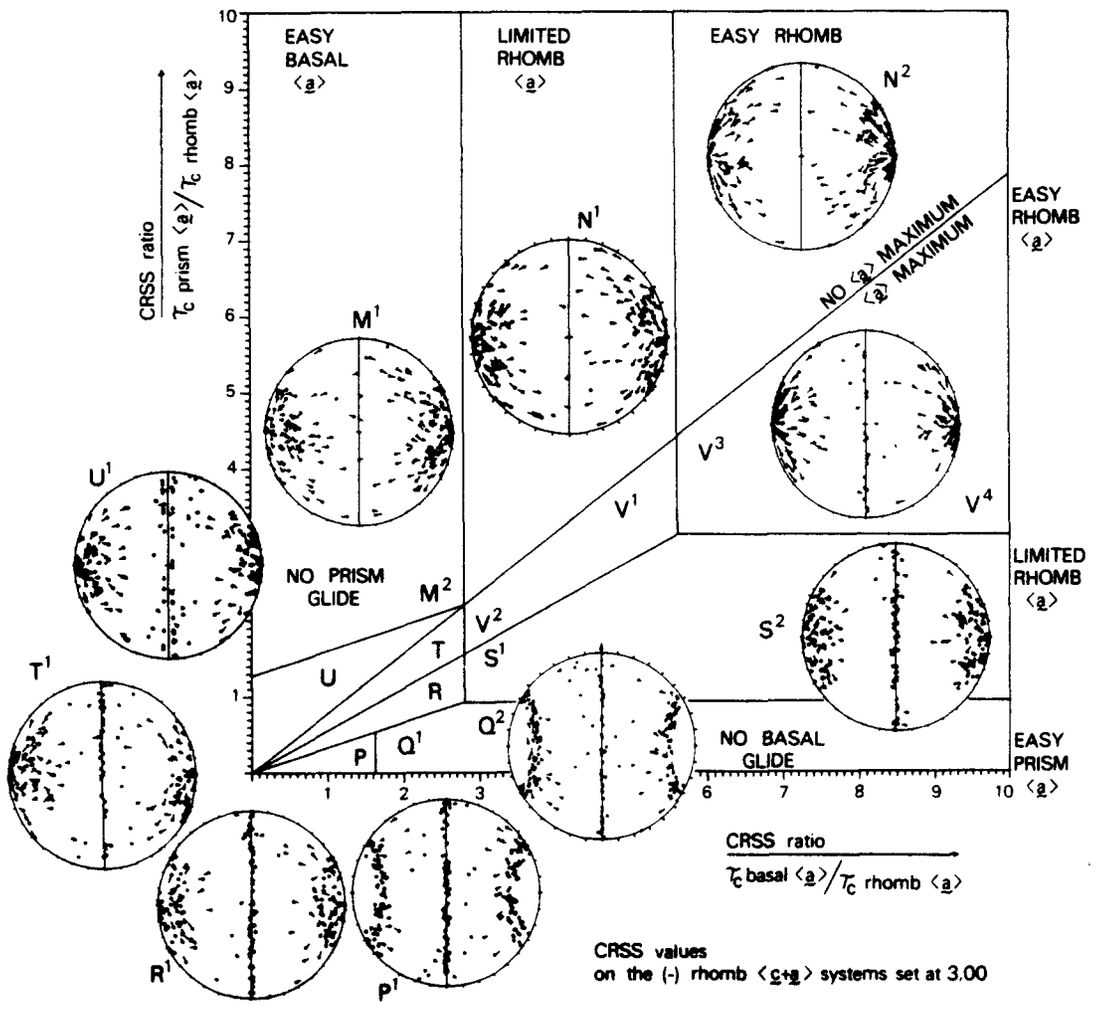

Fig. 12(a)

COMPETITION BETWEEN BASAL AND (−) RHOMB <a> SYSTEMS

The competition between {0001} and {01$\bar{1}$1} <a> systems is rather unusual. The pattern of transition boundaries is related in a straightforward manner to the individual competition between {0001} <a> and {01$\bar{1}$1} <a> systems with the {01$\bar{1}$1} <c + a> systems. The region of CRSS values allowing joint operation of the <a> systems is rather large. Fabric variation is shown for plane strain and axially symmetric shortening (Fig. 11a and b).

SIMULTANEOUS COMPETITION BETWEEN BASAL, PRISM AND RHOMB <a> SYSTEMS

An important simplification of configuration space

Up to this point no more than three individual mechanism sets have been examined at any one time. The configuration spaces have all been two-dimensional, for example plotting the CRSS ratio for {0001} <a>/{01$\bar{1}$1} <c + a> systems against the CRSS ratio for {10$\bar{1}$0} <a>/{01$\bar{1}$1} <c + a> systems. This means that the computer programme should have discovered every one of the possible yield surface configurations in the configuration spaces. Therefore it is possible to make precise statements as to the predictions of the Taylor–Bishop–Hill analysis for total fabric variation with the competitions:

(i) {0001} <a>, {10$\bar{1}$0} <a> and {01$\bar{1}$1} <c + a>;

(ii) {0001} <a>, {01$\bar{1}$1} <a> and {01$\bar{1}$1} <c + a>.

However complex the above transition diagrams may be, they still involve implicit assumptions that the CRSS values on glide systems other than those included are sufficiently high to prevent operation of these additional systems. This may still not be a reasonable assumption, and therefore even more complex configuration spaces must be considered.

Extending configuration space beyond two-dimensions means that there are hundreds of yield surface configurations to be examined, and the task of describing predicted fabric variations becomes correspondingly difficult. Configuration spaces of up to 7 degrees of freedom have been examined but for reasons of space this work will confine itself to reporting

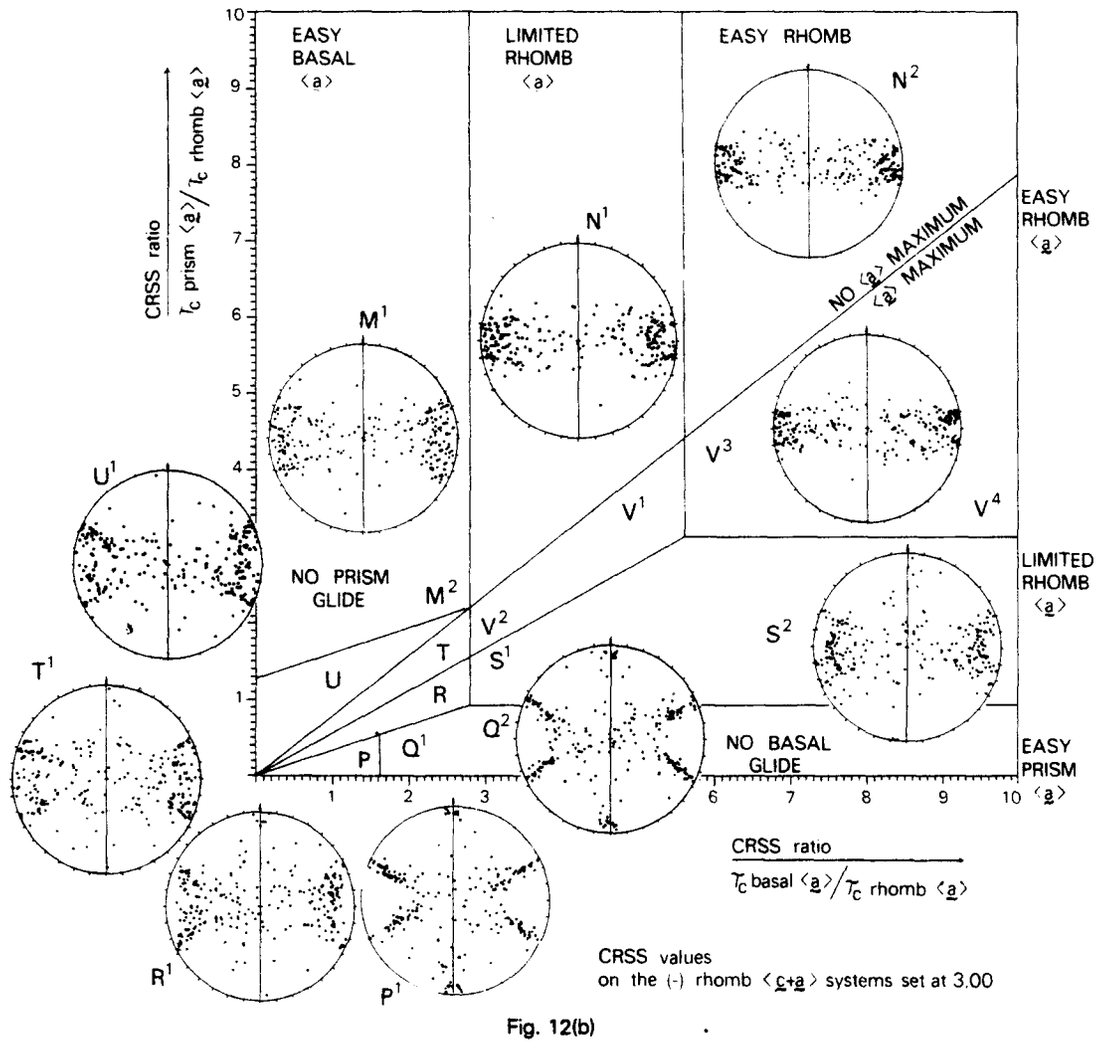

Fig. 12. The transition diagram for the four sets of systems {0001} <*a*>, {10$\bar{1}$0} <*a*>, {01$\bar{1}$1} <*a*> and {01$\bar{1}$1} <*c* + *a*>. The ratios between the CRSS values on <*a*> systems alone determines the competition, and this reduces the 3 degrees of freedom in the competition effectively to 2 degrees. This enables all fabrics for this four-way competition to be portrayed on one two-dimensional diagram. The fabric transitions are illustrated for model quartzites of 250 grains subjected to 65% shortening in (a) axial symmetric shortening and in (b) plane strain. Note the increasing concentrations of c-axes at right-angles to Z as prism glide becomes progressively easier. It should be noted that these diagrams are in fact three-dimensional, since the CRSS value on the <*c* + *a*> systems has also to be considered. However it has been shown that as long as the ratio of CRSS values on the <*a*>/<*c* + *a*> rhomb systems does not exceed 1.4867, the positions of the boundaries on the transition diagram do not change, and the CRSS value on the <*c* + *a*> systems has no influence on fabric development. Only *c*-axis pole figures are shown, as for Fig. 10.

the results of the study of the three-dimensional space defined by the following mechanism subsets:

(i) basal {0001} <*a*>;
(ii) prism {10$\bar{1}$0} <*a*>;
(iii) (−) rhomb {01$\bar{1}$1} <*a*>;
(iv) (−) rhomb {01$\bar{1}$1} <*c* + *a*>.

Once configuration spaces of greater than 2 degrees of freedom are examined, there may be in some corner of the configuration space a yield surface configuration which may produce an interesting fabric, but which is never discovered. It is no longer possible to make precise statements about the total fabric variation predicted by the Taylor–Bishop–Hill analysis because the full range of variation of the effects of different sets of CRSS values has not been fully explored.

This problem would be far more serious, except that it is possible to recognize homeomorphic relations between different two-dimensional sections. These probably result from the linear dependence relations that are possible between <*a*> and <*c* + *a*> systems on the rhomb planes. It has been found that for the two-dimensional sections examined, as long as the CRSS ratio on the (−) rhomb <*a*>/<*c* + *a*> systems does not exceed 1.4867 (the value at which the first transition takes place in the pair-wise competition in Fig. 8), then the CRSS value on the <*c* + *a*> systems has no effect at all on the positions of the transition boundaries, or on the yield surface configuration. Some minor boundaries appear or disappear as the CRSS value on the <*c* + *a*> system is varied, but these boundaries appear to be associated only with trivial changes. This means that, as long as the condition above is obeyed, the yield surface configuration is determined solely by the ratios of the CRSS values for the <*a*> glide systems, and that the CRSS value for the <*c* + *a*> glide systems has no effect at all on fabric development.

The transition diagram for these four systems should be compared with the transition diagram for {0001} <*a*>, {10$\bar{1}$0} <*a*> and {01$\bar{1}$1} <*c* + *a*> systems (Fig. 10). This transition diagram excludes the operation of {01$\bar{1}$1} <*a*> systems and therefore assumes the rhomb <*a*>/<*c* + *a*> CRSS ratio exceeds 2.9738. Figure 10 therefore applies to most of the configuration space for the four sets: {0001} <*a*>, {10$\bar{1}$0} <*a*>, {01$\bar{1}$1} <*a*> and {01$\bar{1}$1} <*c* + *a*> systems. What is interesting is the CRSS limit value for exclusion of {10$\bar{1}$0} <*a*> systems as the CRSS value on the {0001} <*a*> systems drops to zero. With operation of {01$\bar{1}$1} <*a*> systems excluded, this value is defined by a CRSS ratio of 1.9040 on the {10$\bar{1}$1} <*a*>/{01$\bar{1}$0} <*c* + *a*> systems. However, including the rhomb <*a*> systems, allows the prism <*a*> systems to be excluded at progressively lower CRSS ratios. The CRSS limit value for exclusion of prism <*a*> systems is given by the equation:

$$\tau_p \geqslant 0.7800\ \tau_b + 1.2807\ \tau_r,$$

where $\tau_r \leqslant 1.4867\ \tau_k$,

τ_p = CRSS for {10$\bar{1}$0} <*a*> systems,

τ_b = CRSS for {0001} <*a*> systems,

τ_r = CRSS for {01$\bar{1}$0} <*a*> systems and

τ_k = CRSS for {01$\bar{1}$1} <*c* + *a*> systems.

Configurations without rhomb <*a*> can be compared with configurations with rhomb <*a*>. In many cases identical configurations can be located, as far as can be seen by comparison of inverse rotation diagrams for axially symmetric shortening. The rhomb <*a*> systems in these cases can be said to alter the region of CRSS values in which a particular fabric develops, without seeming to affect the fabric. It also means that the same yield surface configuration applies over a very large range of CRSS values. However, as pointed out above, the presence of rhomb <*a*> glide also prevents particular fabrics from developing. These effects mean that the transition diagrams for the four systems {0001}, {10$\bar{1}$0}, {01$\bar{1}$1} <*a*> and {01$\bar{1}$1} <*c* + *a*> can be simply represented. As long as the CRSS ratio on the rhomb <*a*>/<*c* + *a*> systems does not exceed 1.4867, the transition diagram for the above systems has only 2 degrees of freedom. These results were checked for τ_r set at 4.00, 3.00, 1.00 and 0.10 with τ_k = 3.00 (arbitrary units) and hold except for some minor deviations.

The ability to represent fabric variation from four sets of mechanisms on one two-dimensional diagram is a remarkable and unexpected simplification of what appeared to be a rather difficult problem.

The transition diagram is shown in Fig. 12 with the important domains defined. A summary of fabric variation is prepared showing *c*-axis patterns for axially symmetric shortening (Fig. 12a) and for plane strain (Fig. 12b).

RELATIONS BETWEEN DEFORMATION FABRICS AND ENVIRONMENTAL VARIABLES

To some extent, variation in relative CRSS values might allow simulation of different deformation conditions. In this case different regions of configuration space may represent specific environments. There are problems involved in relating CRSS values to real rheological behaviour but some of these can be overcome as long as, for any particular set of environmental variables, there are resolved shear stresses beyond which activity on individual glide systems increases markedly. This means that the mathematically abrupt fabric transitions can be smeared out over a transitional zone.

Although there are no definite functional relations known between yield stresses on various glide systems, some statements can be made about relative strengths. This aspect was discussed briefly by Lister *et al.* (1978). On the basis of experimental work and theoretical considerations, it is expected that the yield stresses for glide systems with long Burgers vectors <*c* + *a*> will be greater than for systems with short vectors. Glide on the basal <*a*> and prism {10$\bar{1}$0} <*a*> systems seem to be the most definitely known deformation mechanisms in quartz, so it is difficult to consider a yield surface configuration as 'realistic' if glide on these two symmetry sets is explicitly excluded by the choice of CRSS values. In this way some restrictions as to the most 'relevant' sections or portions of sections of configuration space can be made.

Certain regions of configuration space will not be relevant to real conditions. For example the experiments of Baeta & Ashbee (1969a, b, 1970a, b) suggest <*c* + *a*> systems are three times harder than <*a*> systems. This supports theoretical arguments (Lister *et al.* 1978) based on the relatively long length of the <*c* + *a*> Burgers vector. Thus regions of configuration space in which CRSS values on <*c* + *a*> systems are relatively high are thought most likely to allow simulation of naturally occurring fabrics. This rule appears to be obeyed.

CONCLUSION

It is difficult to apply the Taylor–Bishop–Hill analysis to quartz. Apart from the obvious physical limitations of the model, there is uncertainty regarding the actual glide systems that operate during natural quartz deformation. The role of the <*c* + *a*> Burgers vector glide systems remains as one of the important but unsolved questions. In applying the analysis it is necessary to specify a list of dislocation glide systems, and so that the Von Mises condition is satisfied, systems with <*c* + *a*> Burgers vector must be included. In reality heterogeneous strain might remove the necessity for the crystal ever to invoke 'hard' glide systems, or alternative deformation mechanisms might operate. An alternative model needs to be formulated. However in terms of developing an understanding of deformation fabrics in quartzite it is useful to attempt to document the predictions of the Taylor–Bishop–Hill analysis, using glide systems discovered by experiments with quartz.

There is a large variation in deformation fabrics predicted by the Taylor–Bishop–Hill analysis for the given

set of dislocation glide systems. This paper characterizes the fabric transitions between some of these fabrics for the following groups of systems:

(i) basal {0001} <**a**>;
(ii) prism {10$\bar{1}$0} <**a**>;
(iii) (−) rhomb {10$\bar{1}$1} <**a**>;
(iv) (−) rhomb {10$\bar{1}$1} <**c** + **a**>.

There are 3 degrees of freedom possible in the assignment of relative CRSS values. However, the problems of exploring such a configuration space have been remarkably simplified by the discovery of homeomorphic relations between different two-dimensional sections of this space, so that all of the fabric variation predicted by the Taylor–Bishop–Hill analysis for this complex system can be represented on relatively few two-dimensional projections.

Different regions of configuration space might be appropriate to simulating the effects of different geological conditions. There are difficulties in relating CRSS values to real rheological behaviour, but some of these problems might be overcome by smearing out the mathematically abrupt fabric transitions. Nevertheless, in a traverse across a metamorphic terrain fabric transitions are likely to take place over short distances, and these transitions should not be taken to necessarily construe abrupt changes in environmental variables. Fabric transitions take place abruptly even when CRSS values vary smoothly. However, if the fabric transition coincides with a major structural element the possibility of a tectonic discontinuity should not be overlooked.

There are several end-orientations for quartz predicted as a result of this work. The actual maxima are determined in orientation, magnitude and intensity distribution by the deformation history and the initial orientation distribution, as well as by the dislocation glide systems active and their relative abilities to operate. However, the concept of end-orientations and the end-orientations predicted lend strong support to the presently out-of-favour concept put forward by Fairbairn (1949) and Sander (1950) that there are several possible discrete and distinct maximum orientations for natural quartz **c**-axis fabrics.

Acknowledgements—This study began at the Australian National University, Canberra, where G. S. Lister was supported by a Research Scholarship. The work continued at The Geological Institute, University of Leiden, The Netherlands, and at the Geology Department of Imperial College, London. Facilities made available by all of these institutions have been invaluable.

All transition diagrams have been calculated by the CDC computer at Petten, The Netherlands, by the courtesy of Dr M. van Hemert, Chemistry Department, Leiden. Other calculations have been performed at the IBM central facility in Leiden.

This work was financed in part by the Netherlands Foundation for Pure Research (Z.W.O.). The development of the technique of growth parameterization used in this study was carried out at Imperial College. G. S. Lister benefited greatly from this assistance and from association with K. McClay, E. Rutter, P. Suddaby and the interactive terminal graphics system of Imperial College.

The assistance of M. Brittijn (drafting), W. Laurijssen (photography) and H. Vogelaar and Lucy van der Wijk (typing) was of great value.

REFERENCES

Baëta, R. D. & Ashbee, K. H. G. 1969a. Slip systems in quartz. I—experiments. *Am. Miner.* **54**, 1551–1573.

Baëta, R. D. & Ashbee, K. H. G. 1969b. Slip systems in quartz. II—interpretation. *Am. Miner.* **54**, 1574–1582.

Baëta, R. D. & Ashbee, K. H. G. 1970a. Mechanical deformation of quartz. I—constant strain rate compression experiments. *Phil. Mag.* **22**, 604–625.

Baëta, R. D. & Ashbee, K. H. G. 1970b. Mechanical deformation of quartz. II—stress relaxation and thermal activation parameters. *Phil. Mag.* **22**, 625–635.

Bhattacharyya, D. S. & Pasayat, S. 1968. Deformation texture in quartz: a theoretical approach. *Tectonophysics* **5**, 303–314.

Bouchez, J.-L. 1977. Plastic deformation of quartzites at low temperature in an area of natural strain gradient. *Tectonophysics* **39**, 25–50.

Calnan, E. A. & Clews, C. J. B. 1950. Deformation textures in face centred cubic metals. *Phil. Mag.* **41**, 1085–1100.

Calnan, E. A. & Clews, C. J. B. 1951a. The development of deformation textures in metals. Part II. Body centred cubic metals. *Phil. Mag.* **42**, 616–635.

Calnan, E. A. & Clews, C. J. B. 1951b. The development of deformation textures in metals. Part III. Hexagonal structures. *Phil. Mag.* **42**, 919–931.

Chin, G. Y. & Mammel, W. L. 1970. Competition among basal, prism and pyramidal slip modes in HCP metals. *Met. Trans.* **1**, 357–361.

Fairbairn, H. W. 1949. *Structural Petrology*. Addison-Wesley, Cambridge, Massachusetts.

Hietanen, A. 1938. Petrology of the Finnish quartzites. *Bull. Commn. géol. Finl.* **122**, 1–118.

Hobbs, B. E., Means, W. D. & Williams, P. F. 1976. *An Outline of Structural Geology*. Wiley, New York.

Hu, H. & Goodman, S. R. 1963. Texture transition in copper. *Trans. metall. Soc. A.I.M.E.* **227**, 627–639.

Kallend, J. S. & Davies, G. J. 1972. A simulation of texture development in FCC metals. *Phil. Mag.* **25**, 471–490.

Leffers, I. 1968. Deformation rate dependence of rolling texture in brass containing 5% zinc. *Scr. Met.* **2**, 447–452.

Lister, G. S., Paterson, M. S. & Hobbs, B. E. 1978. The simulation of fabric development in plastic deformation and its application to quartzite: the model. *Tectonophysics* **45**, 107–158.

Merlini, A. & Beck, P. A. 1955. Effect of zinc content on the rolling texture and annealing texture of alpha-brass. *Trans. metall. Soc. A.I.M.E.* **203**, 385.

Morrison-Smith, D. J., Paterson, M. S. & Hobbs, B. E. 1976. An electron microscope study of plastic deformation in single crystals of synthetic quartz. *Tectonophysics* **33**, 43–50.

Paterson, M. S. 1969. Ductility of rocks. In: *Physics of Strength and Plasticity* (edited by Argon, A. S.) M.I.T. Press, Cambridge, Massachusetts, 377–392.

Sahama, Th.G. 1936. Die Regelung von Quarz und Glimmer in der Gesteinen der Finnisch-Lappländischen Granulit Formation. *Bull. Commn. géol. Finl.* **113**, 119.

Sander, B. 1950. *An Introduction to the Study of Fabrics of Geological Bodies*. Pergamon, Oxford.

Tullis, J. A., Christie, J. M. & Griggs, D. T. 1973. Microstructures and preferred orientations of experimentally deformed quartzites. *Bull. geol. Soc. Am.* **84**, 297–314.

Turner, F. J. & Weiss, L. E. 1963. *Structural Analysis of Metamorphic Tectonites*. McGraw-Hill, New York.

Twiss, R. 1976. Some planar deformation features, slip systems and submicroscopic features in synthetic quartz. *J. Geol.* **84**, 701–724.

Wenk, H. R., Venkitasubramanyan, C. S. & Baker, D. W. 1973. Preferred orientation in experimentally deformed limestone. *Contrib. Mineral. Petrol.* **38**, 81–114.